Copy 44
RM SL58D10

RESEARCH MEMORANDUM

for the

Office of Naval Research

PRELIMINARY TRANSONIC FLUTTER INVESTIGATION OF MODELS OF T-TAIL OF BLACKBURN NA-39 AIRPLANE

By George W. Jones, Jr., and Robert W. Boswinkle, Jr.

Langley Aeronautical Laboratory
Langley Field, Va.

NATIONAL ADVISORY COMMITTEE
FOR AERONAUTICS

WASHINGTON

APR 15 1958

NACA RM SL58D10

NATIONAL ADVISORY COMMITTEE FOR AERONAUTICS

RESEARCH MEMORANDUM

for the

Office of Naval Research

PRELIMINARY TRANSONIC FLUTTER INVESTIGATION OF MODELS OF T-TAIL OF BLACKBURN NA-39 AIRPLANE

By George W. Jones, Jr., and Robert W. Boswinkle, Jr.

SUMMARY

A transonic flutter investigation has been made of models of the T-tail of the Blackburn NA-39 airplane. The models were dynamically and elastically scaled in accordance with criteria which include a flutter safety margin. The investigation is to be considered preliminary in that only estimated airplane properties were available for the scaling. The investigation was made in the Langley transonic blowdown tunnel and covered a Mach number range from 0.71 to 1.15 at simulated altitudes extending to below sea level.

The results of the investigation indicated that, if the models simulated the airplane in all important respects, the airplane would have at least a 32 percent margin of safety in stiffness at sea level at Mach numbers up to 0.90. Symmetric stabilizer pitching oscillations (which may have been symmetric flutter) and antisymmetric flutter were obtained at Mach numbers of about 0.95 and 1.00, respectively, at altitudes as high as about sea level. Near a Mach number of 1.00, a region in which the random tunnel turbulence excited low damped antisymmetric oscillations of the model extended to altitudes above sea level. The relationship to the airplane of the low damped oscillations obtained with the model is not known.

INTRODUCTION

At the request of the Office of Naval Research a transonic flutter investigation has been made of models of the T-tail of the Blackburn NA-39 attack airplane. The T-tail of the airplane consists of an all-movable sweptback stabilizer mounted on top of a sweptback fin. The

incidence of the stabilizer is controlled by hydraulic actuators which rotate the surface about an axis located at about 52 percent of the center-line chord of the stabilizer. The stabilizer is equipped with a two-position, trailing-edge elevator which is locked in the plane of the stabilizer surface at high speeds and is moved to a fixed deflection angle at low speeds. The fin is equipped with an unbalanced trailing-edge rudder which is actuated from an attachment at the bottom end. It is not planned to use viscous dampers on any of the T-tail components of the NA-39 airplane.

Three different types of flutter appeared possible: Antisymmetric flutter of the T-tail as a unit with little or no independent control-surface motion; symmetric flutter of the all-movable horizontal tail; and flutter or "buzz" of the rudder. The possibility of a critical flutter mode involving elevator motion was thought unlikely because the locking device for the elevators was designed to be sufficiently positive so that the elevator frequencies would be very high compared with the other important natural frequencies of the tail. Accordingly, in the models the elevator was made integral with the stabilizer.

The airplane had not yet been constructed when the present project was begun so that measured stiffnesses and natural vibration frequencies were not available for use in scaling the models. Accordingly, computed stiffnesses and masses were used in the model scaling together with criteria which include a flutter safety margin.

The models were investigated in the Langley transonic blowdown tunnel and were mounted so as to simulate the fuselage torsion and side-bending degrees of freedom. The tests were made at Mach numbers from 0.71 to 1.15 at simulated altitudes extending to below sea level.

SYMBOLS

b	semichord of fin or stabilizer, ft
c	local streamwise chord of stabilizer, ft
f	frequency of flutter, cps
l	length scale factor, $\frac{\text{Typical model length}}{\text{Corresponding airplane length}}$
m	mass scale factor, $\frac{\text{Typical model mass}}{\text{Corresponding airplane mass}}$
m'	mass of stabilizer, slugs

M Mach number

q dynamic pressure, lb/sq ft

s value of y at stabilizer tip

t time scale factor,
$$\frac{\text{Time required for tunnel airstream to move 1 model chord length}}{\text{Time required for airplane to move 1 airplane chord length}}$$

T static temperature, $^{\circ}R$

$$v = \frac{\pi}{4}\int_{-s}^{s} c^2\, dy$$

V velocity, ft/sec

$\overline{V}$ reduced velocity based on a representative natural frequency, $\frac{V}{b\omega_i}$

y distance along stabilizer from stabilizer center line, measured perpendicular to stabilizer center line, ft

η nondimensional distance along fin reference axis measured from fin root (see fig. 2)

λ stiffness reduction factor used to provide margin of safety in application of model flutter test results to airplane

μ mass ratio, $\frac{m'}{\rho v}$

ρ static air density, slugs/cu ft

ω_i representative natural frequency, radians/sec

Subscripts:

A airplane

M model

MODELS

Geometry

For this investigation, $\frac{1}{12}$-scale models of the T-tail of the Blackburn NA-39 attack airplane, which is manufactured by Blackburn and General Aircraft, Ltd., were used. A photograph of one of the models is presented as figure 1 and a sketch of the T-tail is shown in figure 2. Some of the more important geometric properties are given in table I.

The stabilizer had an aspect ratio of 2.64, had a taper ratio of 0.582, was swept back 29° along the leading edge and 9° along the trailing edge, and was 5 percent thick. The stabilizer pitch axis was located at about 52 percent of the center-line chord of the stabilizer.

On the airplane the leading edge of the fin is curved and extends forward to the canopy to form a long dorsal fin. On the models the lower part of the fin leading edge was arbitrarily curved downward and terminated as indicated in figures 1 and 2. The fin-rudder trailing edge was swept back 22°. The maximum thickness of the fin-rudder varied from 11 percent at the root to 8 percent at the minimum chord (fig. 2). The leading edge of the main spar of the fin was swept back 27°.

The rudder was located at the trailing edge of the fin and extended over nearly the total fin span. The hinge line was swept back 22°. The rudder chord was constant and was 30.4 percent of the minimum fin-rudder chord, both measured streamwise.

Because of damage to the first model (model 1) during testing, an additional model (model 2) was required for the investigation. The two models were intended to be identical. However, as evidenced by data presented in the section entitled "Physical Properties," there were some differences in the two models. In addition, the sections of the stabilizer for model 1 were not cambered, whereas those for model 2 were inadvertently made with camber. Although the stabilizer sections on the airplane are cambered, the use of models without camber is not thought to affect the flutter results and is preferred because the models usually can be trimmed more easily in the tunnel.

Scaling

In scaling the airplane properties, the nondimensional mass and stiffness distributions were required to be the same for the model as for the airplane. The mass and stiffness levels for the model were

obtained by specifying the scale factors for the fundamental quantities involved: length, mass, and time.

The size of the model was limited by tunnel-wall-interference effects, and on the basis of past experience the length scale factor was chosen to be

$$l = \frac{1}{12} \tag{1}$$

The mass scale factor was obtained from a requirement that the mass ratio μ should be the same for the model as for the airplane, which results in

$$m = \frac{\rho_M}{\rho_A} l^3 \tag{2}$$

In order to locate the simulated sea-level altitude near the middle of the tunnel density range available at a Mach number of 1.00, the density ratio was chosen to be $\rho_M/\rho_A = 1.97$. This location of simulated sea level allows altitudes below sea level to be obtained and flutter margins to be indicated where flutter does not occur above sea level.

The time scale factor was obtained from a requirement that the reduced velocity $\overline{V}$ should be the same for the model as for the airplane, which results in

$$t = \left(\frac{V_M}{V_A}\right)^{-1} l$$

Since the Mach number is the same for the model as for the airplane, the time scale factor may be written

$$t = \left(\frac{T_M}{T_A}\right)^{-1/2} l \tag{3}$$

The static temperature for the airplane T_A is a function only of altitude, and for sea-level altitude it was taken to be 519° R. However, in

the tunnel during a run, the temperature continually drops as air is expended from the reservoir and the temperatures obtained at the various flutter points during an investigation are different. A study of previous flutter data indicated that 408° R was near the average value of the static temperature that would be expected during the present investigation, and this assumed value was used to obtain the temperature ratio used in the scaling: $T_M/T_A = 0.786$.

A list of the pertinent model and flow quantities and the design scale factors used is given in table II. It may be noted that the factor λ is used in the scale factors for some of the quantities listed in table II. The factor λ has the value 0.76 and occurs because the model stiffnesses were made 76 percent of those which would result from application of the scale factors as specified (eqs. (1), (2), and (3)). The purpose of reducing the model stiffnesses was to provide a margin of safety in the application of the model flutter-test results to the airplane. Thus, the design reduced velocity for the model is equal, not to that of the airplane, but to that of an airplane having stiffnesses 76 percent of those of the actual airplane.

The dynamic pressure and Mach number are quantities which are controllable during a run, whereas the temperature is not. If the dynamic pressure and Mach number are considered to be fixed and a static temperature different from the design value is obtained, both the density and velocity will be different from the values considered in the scaling. The density and velocity changes result, respectively, in values of mass ratio and reduced velocity different from the design values. However, a combination of reduced velocity and mass ratio which can be expressed in terms of the dynamic pressure

$$\frac{\bar{V}_M^2}{\mu_M} \propto q_M$$

is independent of the temperature, and this combination is exactly simulated in the runs by the expedient of interpreting the simulated altitude in terms of dynamic pressure. Thus, the scale factor in table II for dynamic pressure is used to convert the dynamic pressure for the airplane at any altitude and Mach number to the dynamic pressure for the model at the same altitude and Mach number. The dynamic pressure for the airplane is assumed to be that calculated by use of the ICAO standard atmosphere (ref. 1). It may be noted that for a given altitude q/M^2 is a constant.

The effect of not satisfying exactly the individual values of mass ratio and reduced velocity is believed to be negligible in the present

investigation. Experience with a wide variety of flutter models has indicated that, at least within the operational limits of the tunnel, flutter at a given Mach number tends to occur at a constant value of dynamic pressure regardless of the individual values of density and velocity.

Construction

Some of the construction details of the models are indicated in the X-ray photographs of figure 3. In construction of the main spars of the stabilizer and of the fin, hollow aluminum-alloy beams of rectangular cross sections were fabricated. Three of the beams were welded together to form the stabilizer spar (fig. 3(b)) and four to form the fin spar (fig. 3(a)); this construction resulted in wide main spars which simulated the multispar arrangement used in the airplane. In the model stabilizer and fin aluminum ribs were welded to the main spar. The leading and trailing edges were pine. Balsa was used to fill the surfaces to contour. Lead weights were placed in the stabilizer at various locations in order to obtain the desired mass distribution. Close simulation of mass distribution was thought to be less important for the fin than for the stabilizer; consequently, no lead weights were used in the fin to correct the fin mass distribution. The rudder was constructed with an aluminum-alloy leading edge and ribs, pine trailing edge, and balsa filler. The various surfaces were wrapped with silk cloth and lacquered. Strain gages were installed on each fin on the main spar near the fin root.

An exploded view of the model components is presented in figure 4. The stabilizer was attached to the fin by a T-shaped fitting at the pitch-axis location and by a U-shaped fitting farther forward. Adjustments in the dimensions and location of the U-shaped fitting provided the desired stiffness between the stabilizer and the fin in the pitching degree of freedom. Adjustments in the dimensions of the T-shaped fitting provided the desired stiffness between the stabilizer and the fin in the rolling and yawing degrees of freedom. The rudder was attached to the fin with two flexure hinges (fig. 3(a)) and the rotational stiffness of the rudder was controlled by a rod which extended down from the hinge line. The rod was welded at the bottom end to a fitting which was attached to the fin root.

The fin was attached to a steel tongue which in turn was attached to a steel flexure fixture (fig. 4). The flexure fixture was designed to simulate the stiffness of the fuselage in side bending and torsion. The flexure fixture was bolted at the upstream end to the two aluminum-alloy parts which are designated in figure 4 as the two sides of the mounting block. The generalized mass of the fuselage was simulated by

the mass of the flexure fixture plus that of a lead weight attached to the flexure fixture and suspended below it.

Physical Properties

The first several natural frequencies and node lines of each of the two models are given in figure 5. Distinct node lines were not obtained for some of the modes, and for these cases the node lines are omitted in the figure. In obtaining the data an electromagnetic shaker was used to excite the model; salt crystals were sprinkled on the surface to define the node lines. Many of the modes were highly coupled and involved motion in several degrees of freedom; therefore, a description of the predominant motions is included in figure 5. Neither measured nor computed natural frequencies and node lines for the airplane were available for comparison with those measured for the models.

The distribution of fin flexibility in torsion and bending for the two models is indicated in figure 6; these data were obtained by applying moments on the stabilizer (yawing moment for torsion and rolling moment for bending) and noting the angular displacements of mirrors attached to the fin along the reference axis (fig. 2). The flexibility of the model fins is also compared in figure 6 with values scaled from those computed for the airplane. Some differences between measured and design values along the fin span are indicated for both torsion and bending for both models 1 and 2. It may be noted that the value of flexibility at the tip is a measure of the overall flexibility. The overall bending flexibility for model 1 (fig. 6(b)) was in good agreement with the scaled design value while the overall torsion flexibility (fig. 6(a)) was in somewhat less agreement. As discussed in the section entitled "Results and Discussion," model 1 was used for only two runs so that the discrepancy in overall torsion flexibility for model 1 is not a serious limitation to the results of the present investigation. The overall torsion flexibility for model 2 (fig. 6(c)) was within 5 percent of the scaled design value, and the overall bending flexibility (fig. 6(d)) was within 8 percent.

The flexibility of the simulated rudder actuator for each model is indicated in table III. As indicated in table III the simulated actuator stiffness for each model agreed closely with the scaled airplane value.

The flexibility in the three angular degrees of freedom of the stabilizer-fin attachment is indicated in table IV along with the ratio of the flexibility in each degree of freedom to the scaled airplane value. The pitch flexibility (reciprocal of stiffness) used for each model is shown to be too low to simulate only one of the hydraulic actuators used on the airplane to vary the stabilizer incidence and too

high to simulate two actuators. (The second actuator on the airplane is not required for the design loads but was specified for safety in the event of malfunctioning of the first actuator.) The roll flexibility for each model simulated very closely the airplane design value. The yaw flexibility was 13 and 7 percent less than the design value for models 1 and 2, respectively.

The design mass properties of the stabilizer sections defined in figure 2 are presented in table V. As described in the section entitled "Construction," lead weights were added to the stabilizer sections in an attempt to give each section the desired mass properties. Table V also contains comparisons of the measured and design values of the overall mass, unbalance about the pitch axis, and moment of inertia about an axis through the stabilizer center of gravity; table VI contains certain comparisons of measured and design values of the moments of inertia about the pitch, roll, and yaw axes. These comparisons indicate at least close overall simulation of the mass properties.

It may be noted that several physical properties which might be of interest are omitted in the present report. These properties include the mass properties of the fin, the rudder, and the simulated fuselage; the torsion flexibility distribution along the rudder span; the bending and torsion flexibility distribution along the stabilizer span; and the torsion and side bending flexibilities of the simulated fuselage. In construction of the models it was considered of primary importance to simulate closely the design mass distribution of the stabilizer and the design flexibility of the fin, the rudder actuator, and the fin stabilizer attachment. Although the model manufacturer made an attempt to simulate the design values of the additional properties of interest, the degree to which these additional properties were simulated has not been determined.

APPARATUS AND TESTS

The investigation was made in the Langley transonic blowdown tunnel which has a slotted test section. The test section is octagonal in cross section and measures $26\frac{1}{4}$ inches between opposite sides. During operation of the tunnel the area of the orifice may be fixed at a given value and, in this case, as the stagnation pressure (and thus the density) is increased, the test-section Mach number increases until the orifice becomes choked. Thereafter, as the stagnation pressure is increased, the Mach number remains approximately constant. However, the area of the orifice may also be varied during a run as the stagnation

pressure is increased so that various operating paths of Mach number and density may be followed. Both methods of operation were used in the present investigation.

The static-density range is approximately 0.001 to 0.012 slug per cubic foot and Mach numbers from subsonic values to a maximum of about 1.4 may be obtained. It should be noted that because of the expansion of the air in the reservoir during a run, the stagnation temperature continually decreases so that the test-section velocity is not uniquely defined by the Mach number. Additional details of the tunnel are contained in reference 2. Excellent agreement between flutter data obtained in the tunnel and in free air has been observed (ref. 3).

In this investigation the model was mounted on a sting which formed a fuselage that extended upstream into the subsonic flow region of the tunnel (fig. 7). This arrangement prevented the formation of shock waves off the fuselage nose which might reflect from the tunnel walls onto the model. The sting consisted of two 3-inch-diameter tubes fitted one above the other as indicated in figure 7. The upper tube accommodated the fuselage block (fig. 4) and the lower tube shielded the lead weight which was suspended from the fuselage flexibility fixture (fig. 4). The sting and model weighed approximately 310 pounds, and the system had a fundamental bending frequency of about 15 cycles per second.

Wire strain gages were mounted on the main spar of the fin near the root (fig. 3(a)) and were oriented to indicate fin deflections about two different axes. The stabilizer was not equipped with strain gages. A strain gage was installed to indicate rotation of the rudder but the installation was faulty and no information was obtained from this instrumentation. The strain-gage signals, the tunnel stagnation and static pressure, and the stagnation temperature were recorded on a recording oscillograph. The strain-gage signals were used to indicate the start of antisymmetric flutter and the flutter frequency. High-speed motion pictures were made during the runs.

An optical system displayed an image of the model on a ground-glass screen during the runs. The image was watched carefully in an attempt to observe flutter and to stop the air flow before the model became damaged. As a further aid in detecting flutter, the outputs of the strain gages oriented along the two axes of the fin spar were fed across the two plates of an oscilloscope and the onset of flutter was indicated by the formation of a simple Lissajous figure on the scope. The strain-gage outputs were also viewed on the recording oscillograph.

Since the models had somewhat less than scaled strength, it was necessary to orient them with the tunnel airstream in order to avoid excessive static loadings that might destroy the models. The model

was considered to be trimmed in angle of attack when zero symmetric deflection of the stabilizer tips was observed and to be trimmed in angle of yaw when zero antisymmetric deflection of the stabilizer tips was observed. Several trim runs were required to determine the proper orientation of the model.

RESULTS AND DISCUSSION

Interpretation of Results

As stated in the section entitled "Scaling," the model stiffnesses were 76 percent of the scaled airplane stiffnesses. The simulated altitudes which are indicated in figure 9 are thus to be interpreted as altitudes which, if cleared by the model, could be reached with a 32 percent $\left(\frac{1}{0.76} = 1.32\right)$ margin of safety in stiffness by the airplane. This statement assumes, of course, that the model in all other respects exactly simulates the airplane. An alternate interpretation of the results is that a flutter point obtained with the model indicates that the airplane will flutter at the same Mach number at a simulated altitude corresponding to a dynamic pressure 32 percent higher than that for the model.

Presentation of Data

The results of the investigation are presented in table VII. It may be noted that several data points are tabulated for some of the runs. These points are listed in chronological order and each point is plotted in figure 8. Lines in figure 8 connecting the various data points for a given run indicate the dynamic-pressure—Mach number path followed during that portion of the run. The remaining portions of the paths have been omitted in figure 8.

During some of the runs intermittent bursts of nearly sinusoidal oscillations were obtained. It is believed that for this condition the damping was low but not zero. Selection of these low damping conditions from the oscillograph records was somewhat arbitrary because the start of low damping was indefinite. The regions selected are indicated in table VII and figure 8 as "low damping."

As noted in figure 8, model 1 was used for runs 2 and 3. The model was damaged at the dynamic pressure and Mach number indicated by the upper datum point for run 3. The model failure was not due to flutter. It is believed that the model was not trimmed and that the failure was

caused by excessive loads. Considerably more time was spent in orienting model 2 and this model survived runs 5 to 11 and was damaged in run 12 by flutter.

As indicated in figure 8, both antisymmetric flutter and symmetric oscillations were obtained in the tests. The antisymmetric flutter was indicated by the strain-gage traces which were recorded simultaneously with the tunnel pressures and temperature; consequently, the dynamic pressure and Mach number at which antisymmetric flutter occurred are known rather accurately. However, strain gages were located only on the fin where they would not respond to symmetric oscillations of the stabilizer. The evidence of symmetric oscillations, which might have been symmetric flutter, was obtained from the high-speed motion pictures. Since there was no continuous correlation of time on the motion-picture film with time on the oscillograph record, some estimating was necessary to select the points on the oscillograph record which corresponded to the start and stop of symmetric oscillations on the film. Consequently, the data are known with less accuracy for the symmetric oscillations than for antisymmetric flutter.

The data in table VII and figure 8 are summarized in figure 9. Simulated altitude curves in figure 9 are shown for sea level and 10,000 feet. It may be noted in figure 9 that the airplane flight boundary consists of flight at sea level to a Mach number of 0.98 and thereafter of flight at a constant dynamic pressure to the maximum Mach number of 1.05.

Discussion of Results

No flutter was obtained (figs. 8 and 9) at altitudes as low as sea level at Mach numbers up to 0.9. These results indicate that, if the models simulated the airplane in all important respects, the airplane would have at least a 32 percent margin of safety in stiffness at sea level at Mach numbers up to 0.9.

The region for symmetric stabilizer pitching oscillations (which may have been flutter) was located at a Mach number of about 0.95 and extended to altitudes as high as sea level. Additional flutter tests would be required to determine the gravity of this oscillation mode and to determine its boundary.

The region for antisymmetric flutter, which involved yawing and rolling of the stabilizer, extended to altitudes as high as about sea level at a Mach number of 1.00. However, a region in which the random tunnel turbulence excited low damped antisymmetric oscillations of the model extended to altitudes above sea level. The beginning of the low

damped oscillations was indefinite and the choice of a point on an oscillograph record where the oscillations were said to begin was made rather arbitrarily. The relationship to the airplane of the low damped oscillations obtained with the model is not known.

The lower part of the fin leading edge (fig. 1) extended forward some distance ahead of the stabilizer, and the possibility exists that shock waves from the fin could reflect from the walls back to the model at Mach numbers above 1.00 so that the data obtained above a Mach number of 1.00 may be open to some question.

In any extension of the present preliminary investigation, wherein measured airplane properties would be used to scale the models, it is recommended that the stabilizer be provided with instruments to detect symmetric flutter more directly than with motion-picture records. The rudder should also be provided with instruments to indicate rudder oscillations.

CONCLUSIONS

A preliminary transonic flutter investigation of models of the T-tail of the Blackburn and General Aircraft, Ltd., NA-39 airplane has indicated the following conclusions:

1. If the models simulated the airplane in all important respects, the airplane would have at least a 32 percent margin of safety in stiffness at sea level at Mach numbers up to 0.9.

2. Symmetric stabilizer pitching oscillations (which may have been symmetric flutter) and antisymmetric flutter were obtained at Mach numbers of about 0.95 and 1.0, respectively, at altitudes as high as about sea level.

3. Near a Mach number of 1.00, a region in which the random tunnel turbulence excited low damped antisymmetric oscillations of the model extended to altitudes above sea level. The relationship to the airplane of the low damped oscillations obtained with the model is not known.

Langley Aeronautical Laboratory,
National Advisory Committee for Aeronautics,
Langley Field, Va., March 21, 1958.

REFERENCES

1. Anon: Standard Atmosphere - Tables and Data for Altitudes to 65,800 Feet. NACA Rep. 1235, 1955. (Supersedes NACA TN 3182.)

2. Unangst, John R., and Jones, George W., Jr.: Some Effects of Sweep and Aspect Ratio on the Transonic Flutter Characteristics of a Series of Thin Cantilever Wings Having a Taper Ratio of 0.6. NACA RM L55I13a, 1956.

3. Bursnall, William J.: Initial Flutter Tests in the Langley Transonic Blowdown Tunnel and Comparison With Free-Flight Flutter Results. NACA RM L52K14, 1953.

TABLE I.- GEOMETRIC CHARACTERISTICS OF MODELS

Stabilizer:	
Aspect ratio	2.64
Sweepback of leading edge, deg	29
Sweepback of trailing edge, deg	9
Taper ratio	0.582
Maximum thickness at center line, percent center-line chord	5
Maximum thickness at tip, percent streamwise tip chord	5
Center-line chord, ft	0.559
Span, ft	1.170
Area, sq ft	0.518
Pitch axis, percent center-line chord	52
Fin-rudder:	
Sweepback of trailing edge, deg	22
Maximum root thickness, percent streamwise root chord	11
Maximum thickness at minimum streamwise chord, percent minimum streamwise chord	8
Streamwise root chord, ft	1.08
Minimum streamwise chord, ft	0.56
Area, sq ft	0.45
Height of stabilizer above fin-rudder root chord, ft	0.57
Sweepback of leading edge of main spar, deg	27
Rudder:	
Sweepback of hinge line, deg	22
Streamwise chord, ft	0.17
Rudder span (perpendicular to fuselage center line), ft	0.45
Area, sq ft	0.076
Fuselage:	
Diameter, ft	0.25

TABLE II.- DESIGN SCALE FACTORS OF PERTINENT

MODEL AND FLOW QUANTITIES

$$\left[\frac{\rho_M}{\rho_A} = 1.97 \qquad \frac{T_M}{T_A} = 0.786 \qquad \lambda = 0.760\right]$$

Quantity	Design scale factor	
	Symbolical	Numerical
Fundamental quantities:		
Length	l	$\frac{1}{12}$
Mass	$m = \left(\frac{\rho_M}{\rho_A}\right) l^3$	1.14×10^{-3}
Time	$t = \left(\frac{T_M}{T_A}\right)^{-0.5} l$	0.940×10^{-1}
Derived quantities:		
Stream velocity	lt^{-1}	0.887
Stream dynamic pressure	$ml^{-1}t^{-2}$	1.55
Moment of inertia	ml^2	0.792×10^{-5}
Natural vibration frequencies	$\lambda^{0.5}t^{-1}$	9.27
Angular deflections per unit applied moment	$\lambda^{-1}l^{-2}m^{-1}t^2$	1470

TABLE III.- RELATIVE ANGULAR DEFLECTION BETWEEN RUDDER AND FIN PER UNIT APPLIED MOMENT IN RUDDER-ROTATION DEGREE OF FREEDOM FOR MODELS 1 AND 2

Model	Relative angular deflection per unit applied moment, radians/ft-lb	Relative angular deflection per unit applied moment divided by design value
1	0.0869	0.976
2	.0877	.984

TABLE IV.- RELATIVE ANGULAR DEFLECTION BETWEEN STABILIZER AND FIN PER UNIT APPLIED MOMENT IN VARIOUS DEGREES OF FREEDOM FOR MODELS 1 AND 2

Model	Degree of freedom	Relative angular deflection per unit applied moment, radians/ft-lb	Relative angular deflection per unit applied moment divided by design value
1	Pitch	5.2×10^{-4}	[a] 0.67 [b] 1.34
	Roll	4.8	1.01
	Yaw	8.0	.87
2	Pitch	4.9×10^{-4}	[a] 0.62 [b] 1.24
	Roll	4.7	.99
	Yaw	8.5	.93

[a] Based on one pitch actuator.
[b] Based on two pitch actuators.

TABLE V.- MASS PROPERTIES OF STABILIZER SECTIONS

INCLUDING STABILIZER FAIRING

Section (defined in fig. 2)	Mass, slugs	Unbalance about pitch axis, positive for center of gravity rearward of pitch axis, slug-ft	Moment of inertia about axis through section center of gravity and perpendicular to plane of symmetry, slug-ft^2
Design			
1	4.25×10^{-3}	-0.80×10^{-4}	8.45×10^{-5}
2	1.91	.01	2.92
3	1.68	.74	2.11
4	1.46	1.35	1.48
5	1.08	1.57	.87
Whole stabilizer	20.76	5.74	38.17
Ratio of measured to design values for model 2			
Whole stabilizer	0.997	0.993	1.074

TABLE VI.- COMPARISON OF DESIGN AND MEASURED MOMENTS OF INERTIA

OF WHOLE STABILIZER INCLUDING STABILIZER FAIRING

Moment of inertia about indicated degree-of-freedom axis		
Pitch	Roll	Yaw
Design, slug-ft^2		
0.397×10^{-3}	1.516×10^{-3}	1.913×10^{-3}
Ratio of measured to design values		
1.107	1.055	1.045

TABLE VII.- COMPILATION OF FLUTTER DATA

Model	Run	Point	Model behavior (a)	f, cps	M	q, lb/sq ft	V, ft/sec	ρ, slugs/cu ft	T, °R
1	2	1	N	--	0.709	1,300	736	0.0048	448
		2	N	--	.729	1,416	747	.0051	437
	3	1	N	--	.815	1,656	843	.0046	446
		2	N	--	.819	1,862	840	.0053	437
2	5	1	N	--	.848	1,264	872	.0033	440
		2	N	--	.901	1,475	914	.0035	428
	6	1	N	--	1.044	1,722	1,036	.0032	410
		2	N	--	1.078	1,968	1,056	.0035	399
	7	1	N	--	.951	1,583	965	.0034	428
		2	N	--	.966	1,827	967	.0039	417
	8	1	N	--	.796	1,178	836	.0034	459
		2	N	--	.864	1,375	895	.0034	447
		3	N	--	.978	1,745	993	.0035	429
		4	D	--	1.049	1,966	1,047	.0036	414
		5	D_E	--	1.087	2,088	1,077	.0036	409
		6	D	--	1.119	2,213	1,097	.0037	400
		7	D_E	--	1.146	2,294	1,117	.0037	395
	9	1	N	--	.775	1,417	814	.0043	460
		2	N	--	.877	1,787	904	.0044	442
		3	S	--	.943	2,032	958	.0044	430
		4	S_E	--	.955	2,066	968	.0044	427
		5	D	--	.980	2,193	988	.0045	423
		6	D	--	1.013	2,383	1,009	.0047	413
		7	D_E	--	1.090	2,380	1,060	.0042	394
		8	N	--	1.101	2,383	1,065	.0042	390
	10	1	N	--	.815	1,693	850	.0047	452
		2	N	--	.906	2,016	928	.0047	437
		3	S	--	.948	2,173	960	.0047	427
		4	S_E	--	.966	2,255	974	.0047	424
		5	A	62	.989	2,382	994	.0048	420
		6	A_E-D	--	1.032	2,595	1,024	.0049	410
		7	D_E-A	61	1.040	2,657	1,030	.0050	409
		8	A_E	--	1.058	2,726	1,041	.0050	403
		9	N	--	1.074	2,768	1,052	.0050	400
	11	1	N	--	.968	1,824	991	.0037	436
		2	D	--	.983	2,098	996	.0042	427
		3	D_E-A	63	1.004	2,399	1,005	.0048	417
		4	A_E-D	--	.999	2,413	999	.0048	416
		5	D_E-A	61	.998	2,445	997	.0049	415
		6	A_E	--	.996	2,452	994	.0050	415
		7	N	--	.985	2,418	983	.0050	415
	12	1	N	--	.917	1,836	958	.0040	454
		2	N	--	.921	2,300	954	.0050	447
		3	N	--	.895	2,339	925	.0055	445
		4	S	--	.917	2,501	942	.0056	439
		5	S_E	--	.934	2,612	955	.0057	435
		6	A	61	.953	2,772	972	.0059	433
		7	A	--	.979	2,978	990	.0061	425

(a) Model behavior code: N - no flutter, D - start or continuation of low damping, D_E - end of low damping, S - start of symmetric oscillations, S_E - end of symmetric oscillations, A - start or continuation of antisymmetric flutter, A_E - end of antisymmetric flutter.

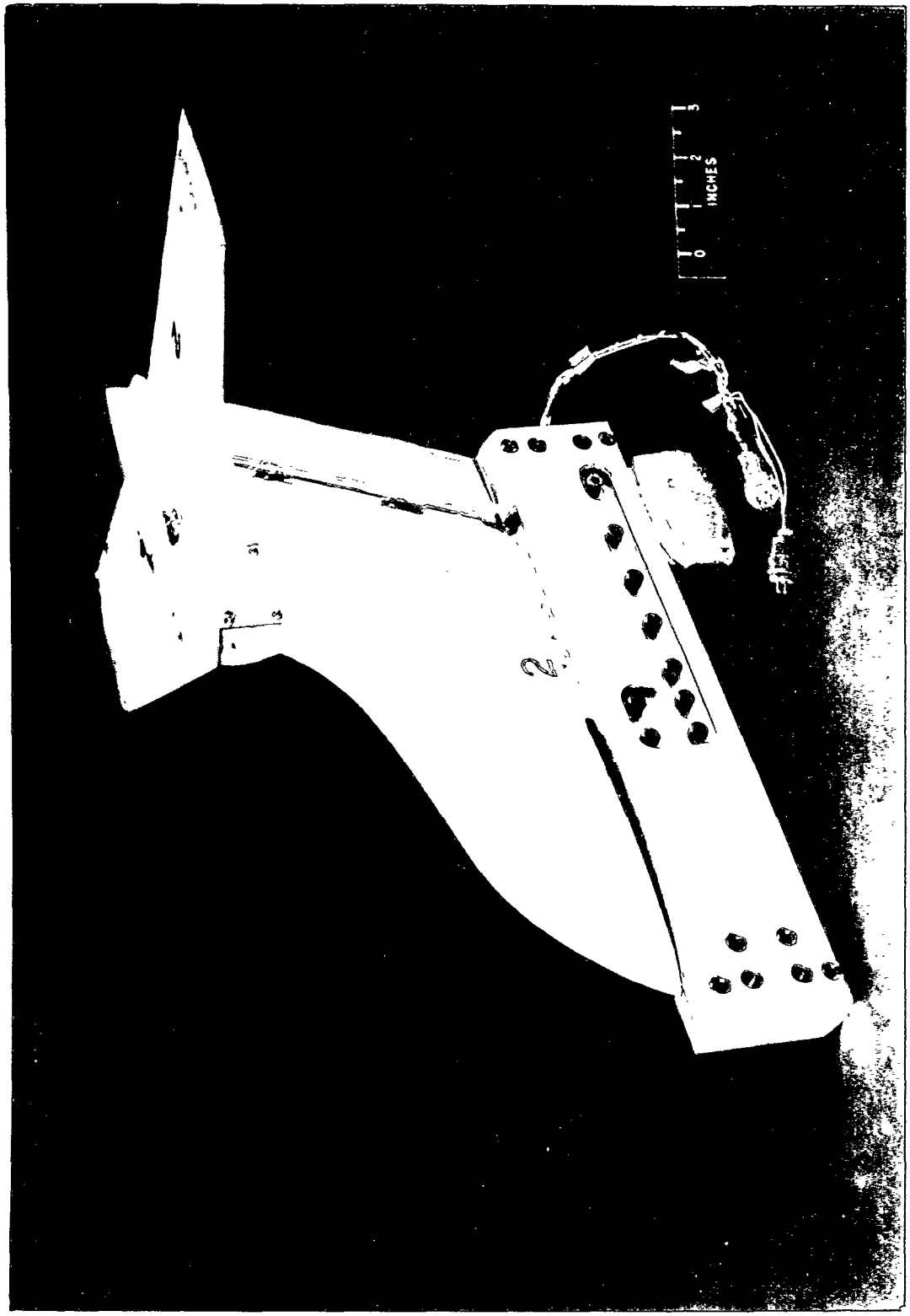

Figure 1.- Model in mounting block. L-57-5008

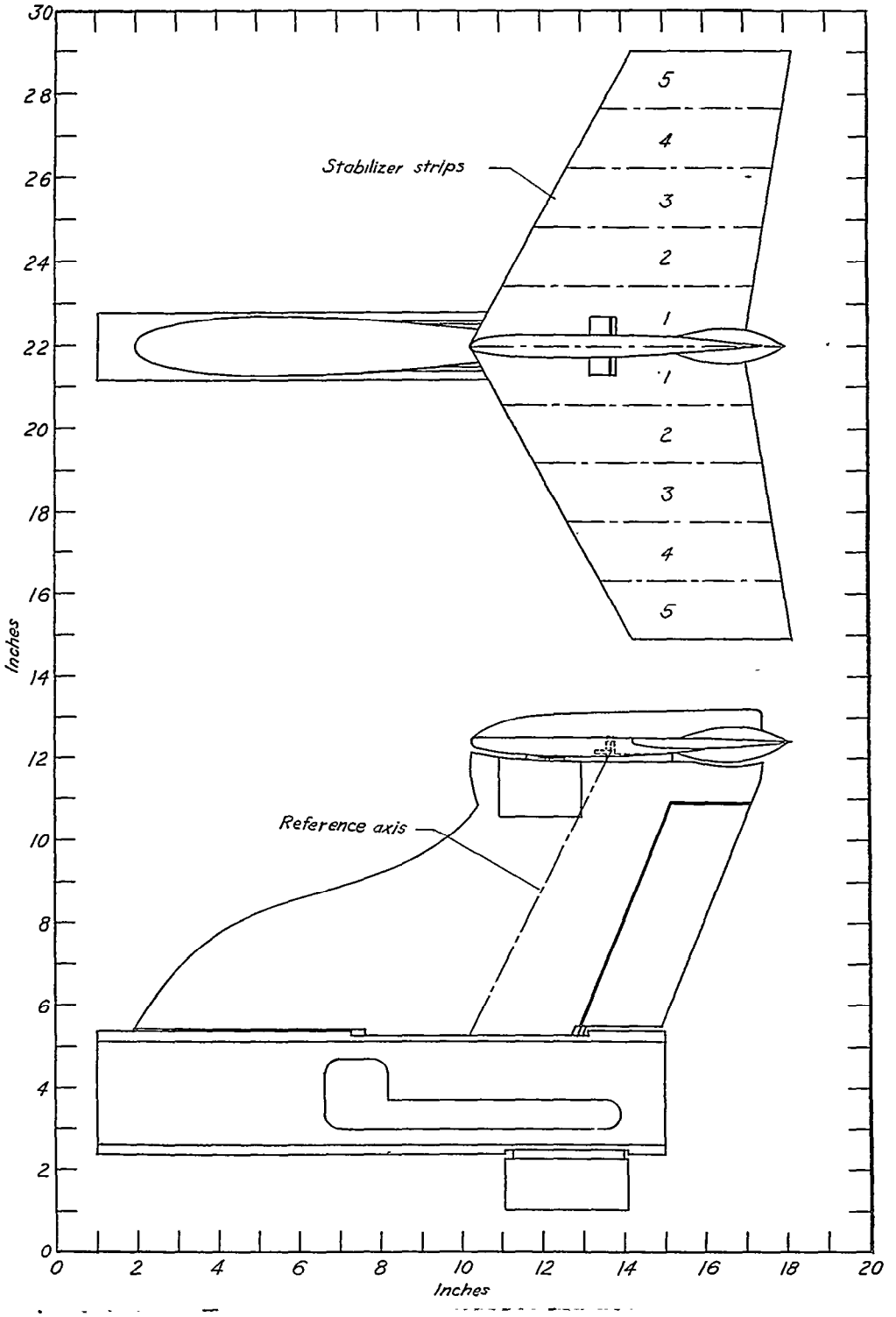

Figure 2.- Sketch of model.

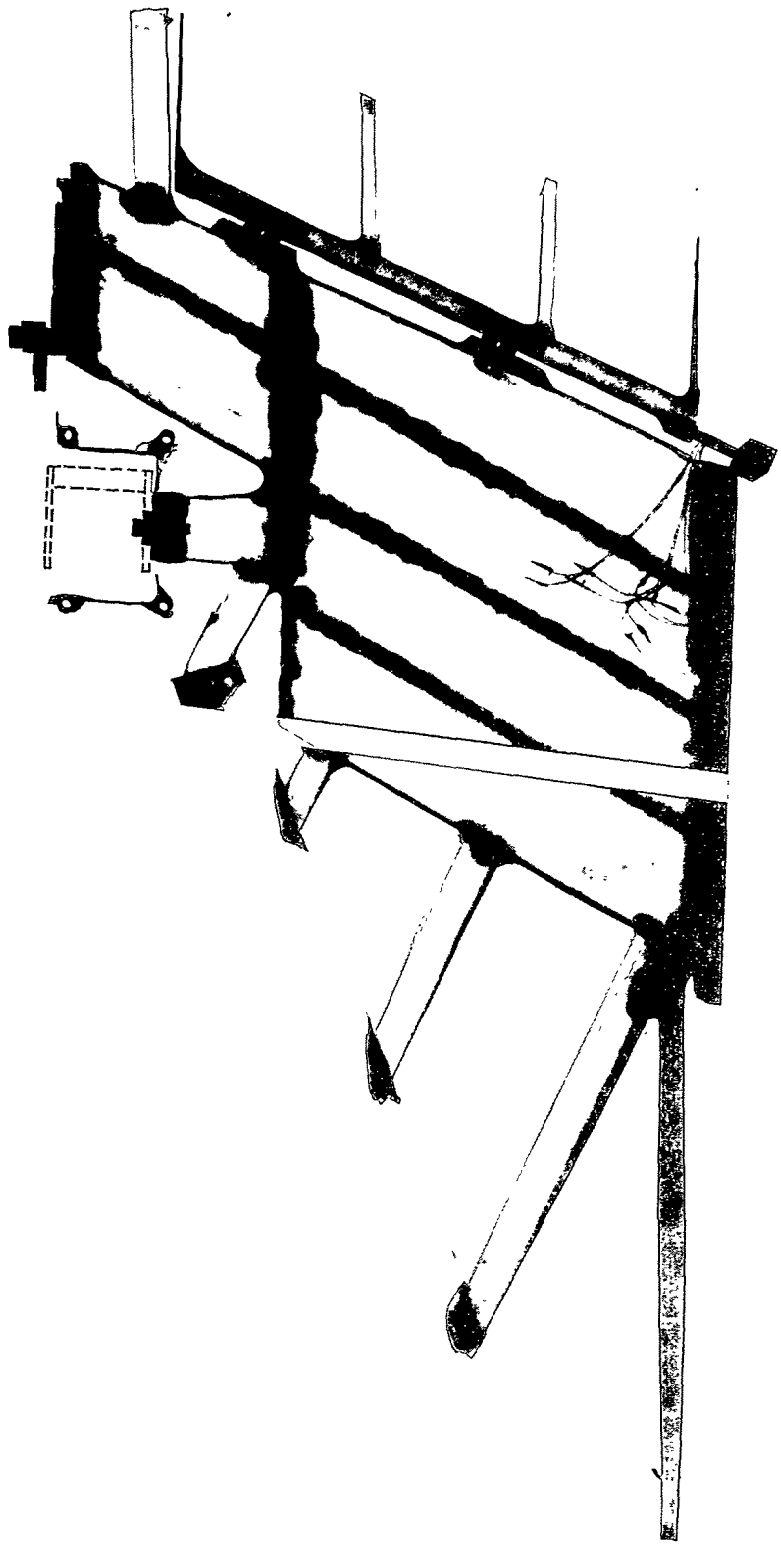

(a) Fin and rudder. L-58-188

Figure 3.- Composite X-ray photographs of model.

(b) Stabilizer. L-58-189

Figure 3.- Concluded.

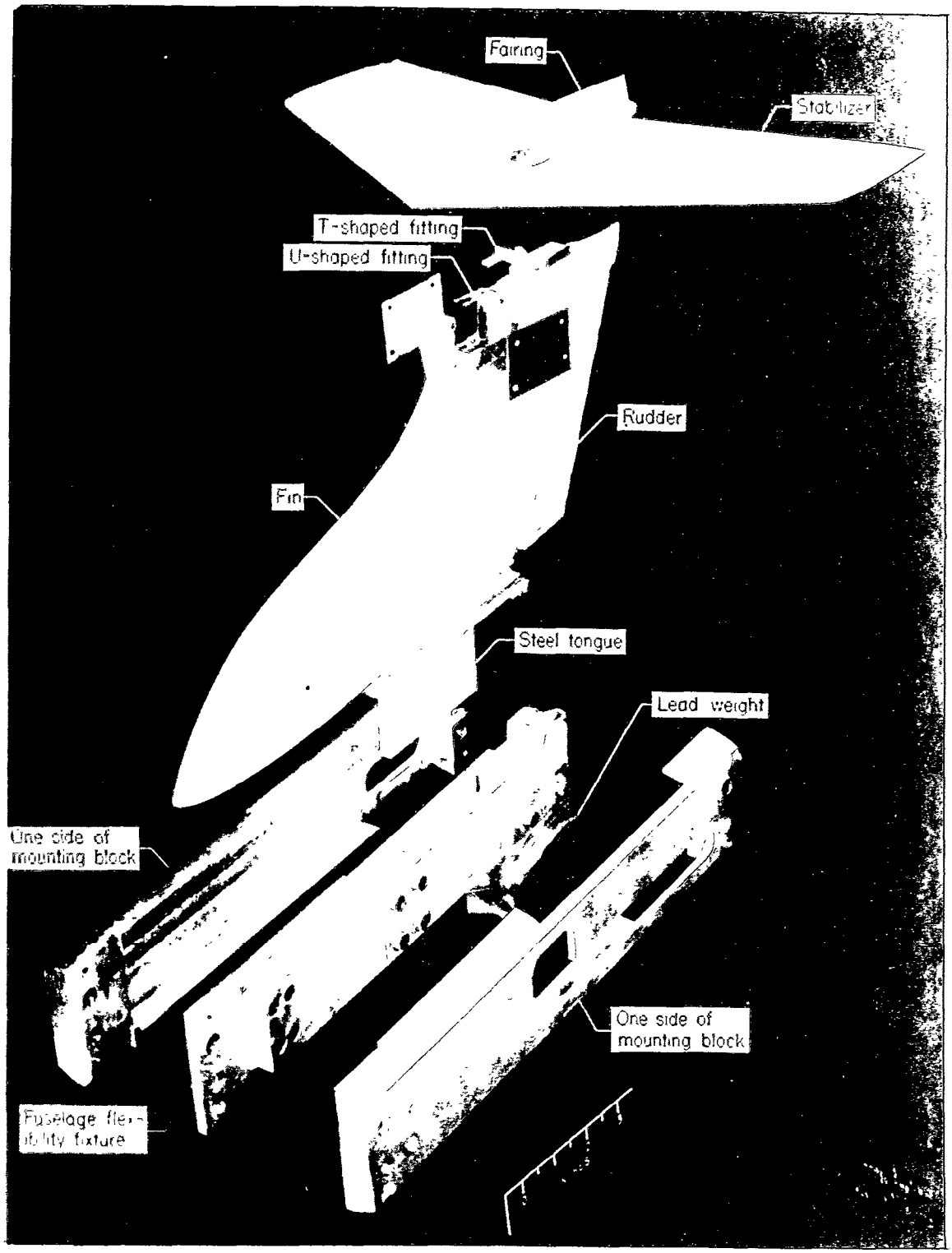

Figure 4.- Exploded view of model. L-57-5190

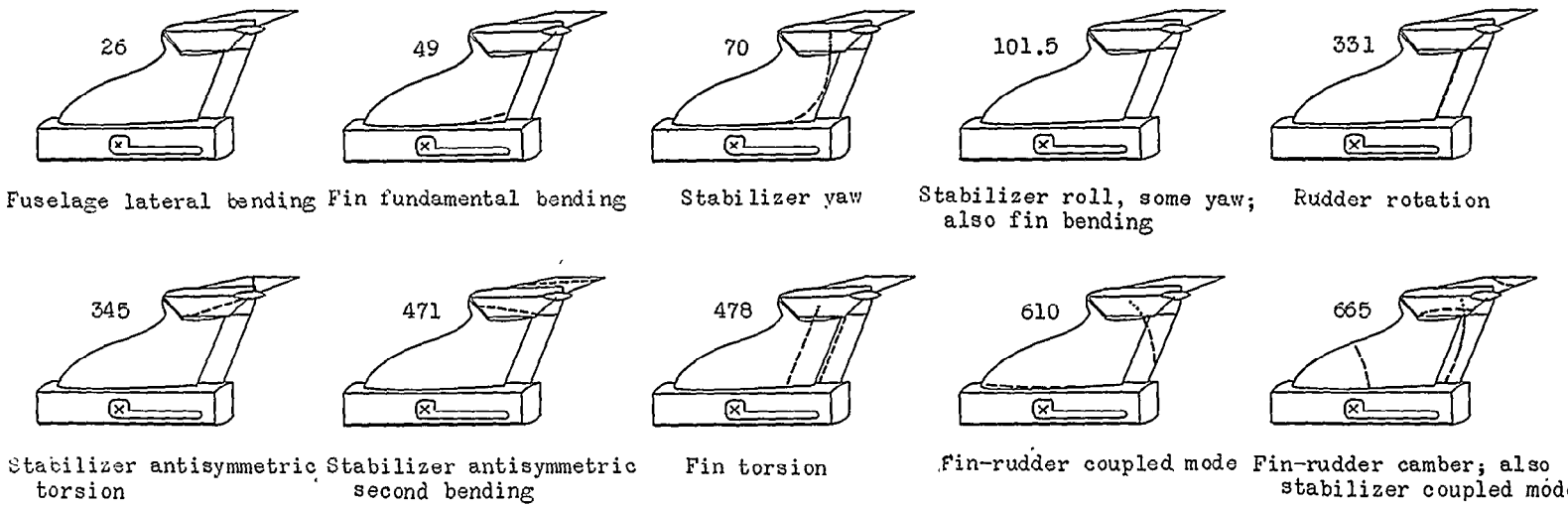

(a) Model 1, antisymmetric modes.

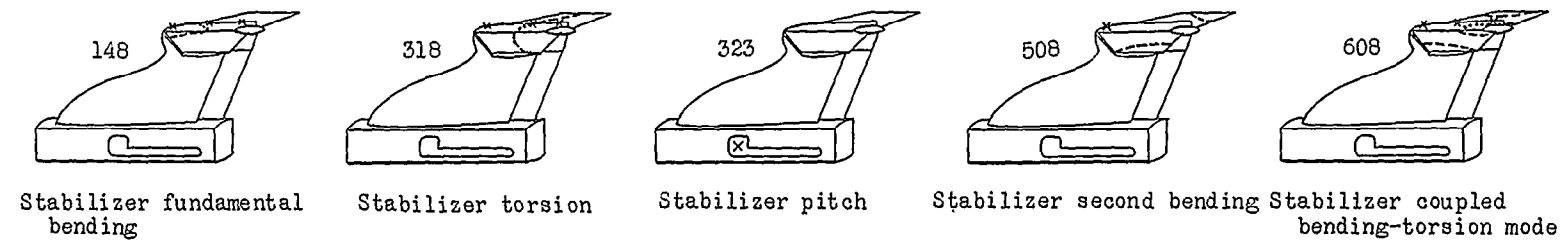

(b) Model 1, symmetric modes.

Figure 5.- Measured natural vibration frequencies (cps) and node lines of the model. The letter X denotes shaker location, dashed lines indicate node lines, and dotted lines indicate invisible portion of node lines.

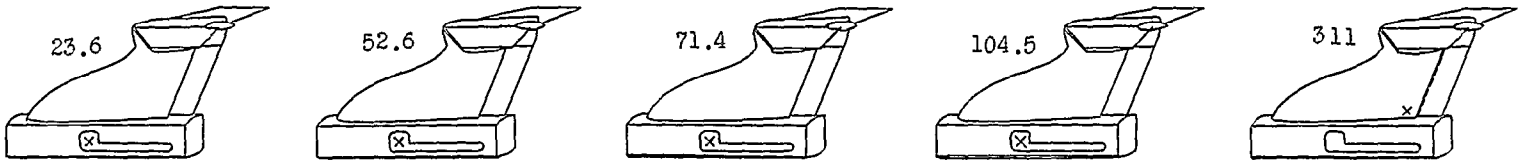

Fuselage lateral bending | Fin fundamental bending | Stabilizer yaw | Stabilizer roll, some yaw; also fin bending | Rudder rotation

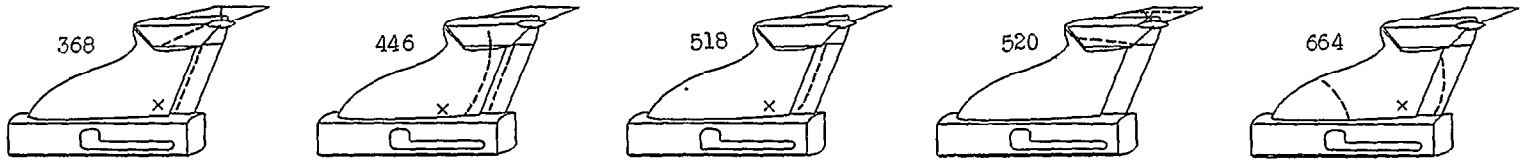

Stabilizer antisymmetric torsion; also rudder rotation | Fin torsion | Camber bending of rudder | Stabilizer antisymmetric second bending | Fin-rudder camber bending

(c) Model 2, antisymmetric modes.

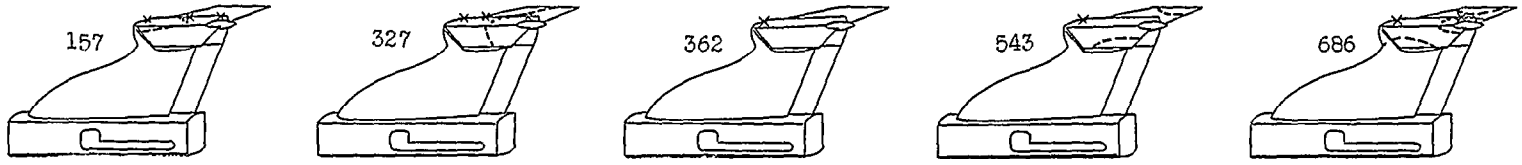

Stabilizer fundamental bending | Stabilizer torsion | Stabilizer pitch | Stabilizer second bending | Stabilizer coupled bending-torsion mode

(d) Model 2, symmetric modes.

Figure 5.- Concluded.

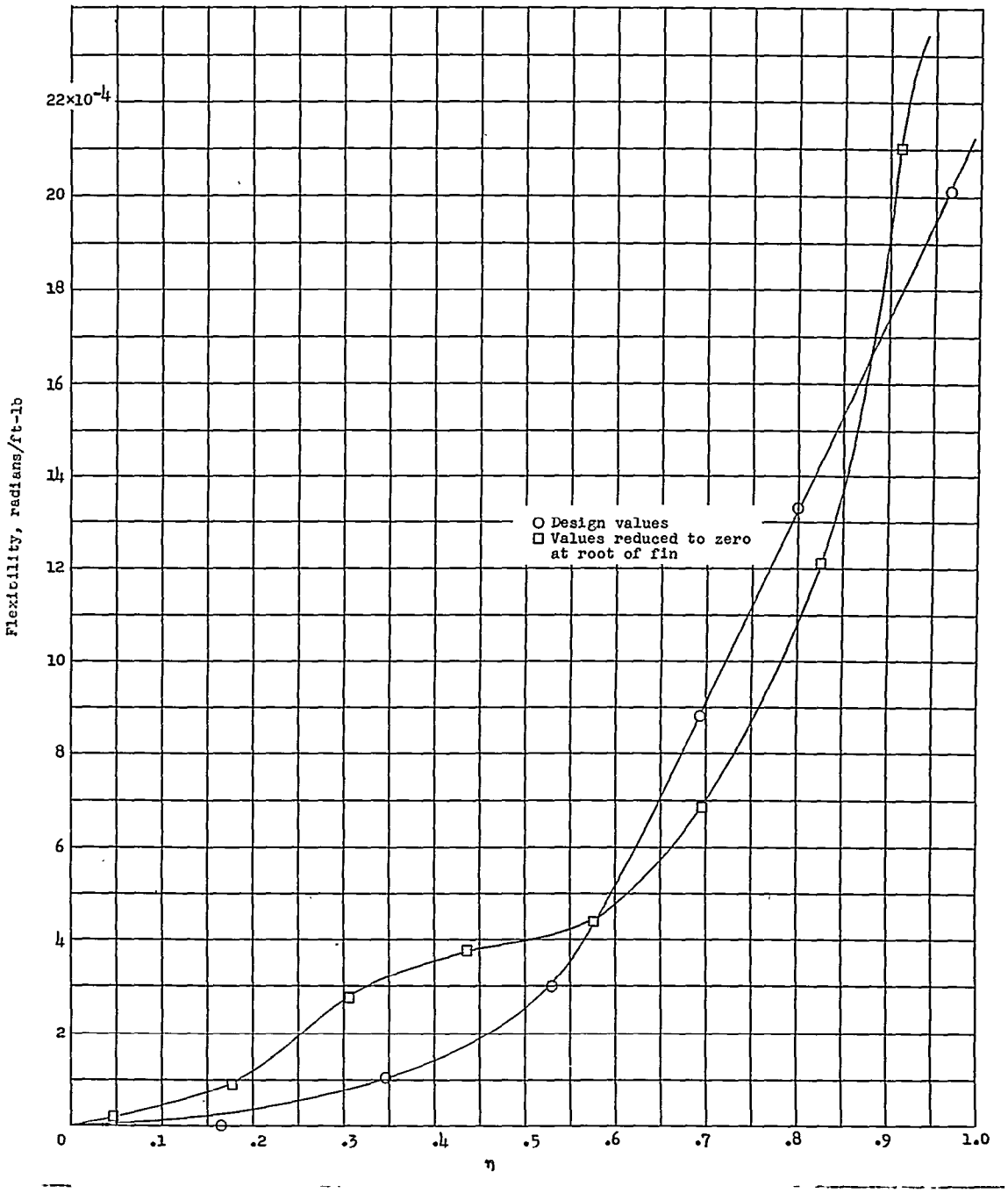

(a) Angular torsion deflection of fin per unit yawing moment applied to stabilizer, model 1.

Figure 6.- Comparison of design and measured torsion and bending fin flexibilities.

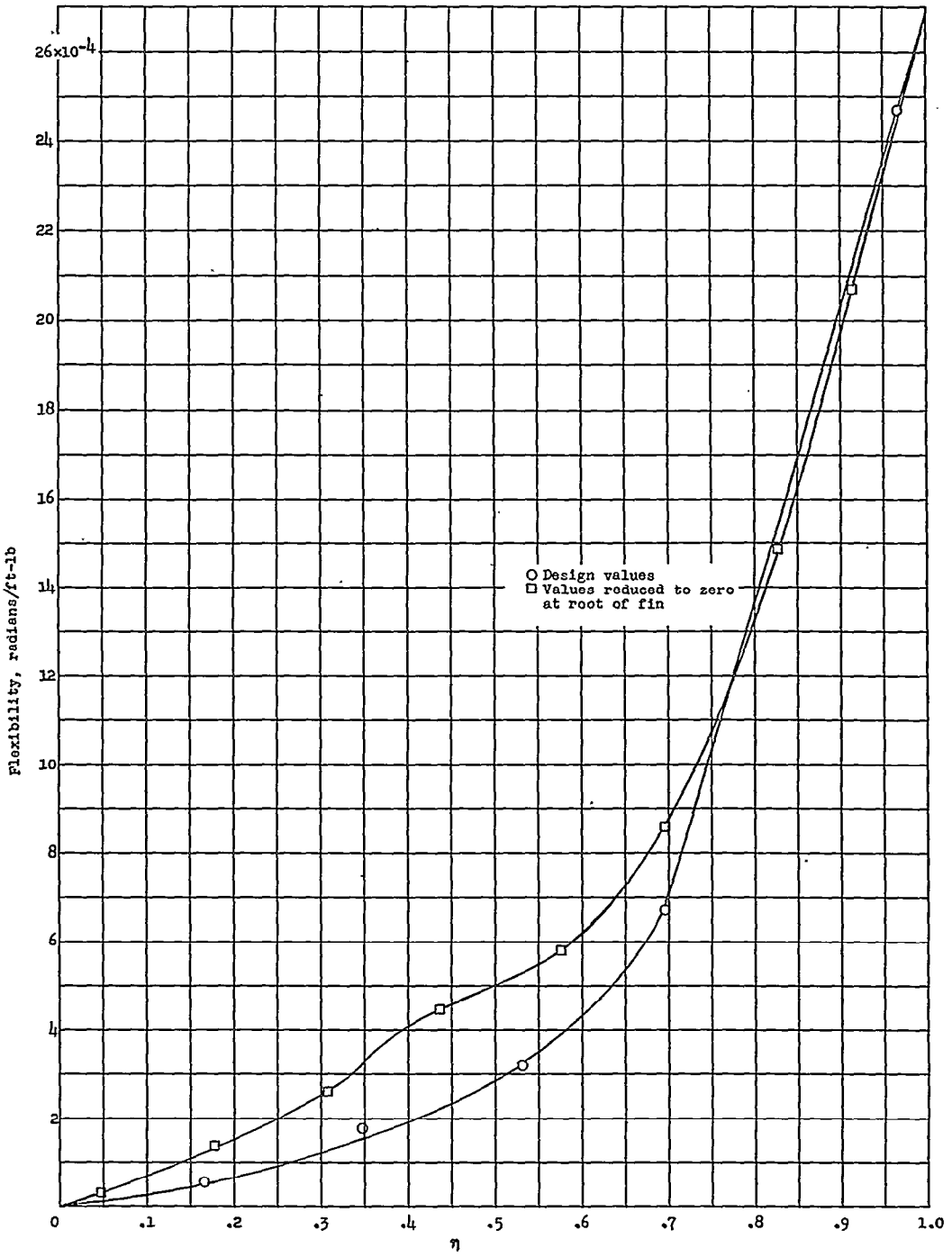

(b) Angular bending deflection of fin per unit rolling moment applied to stabilizer, model 1.

Figure 6.- Continued.

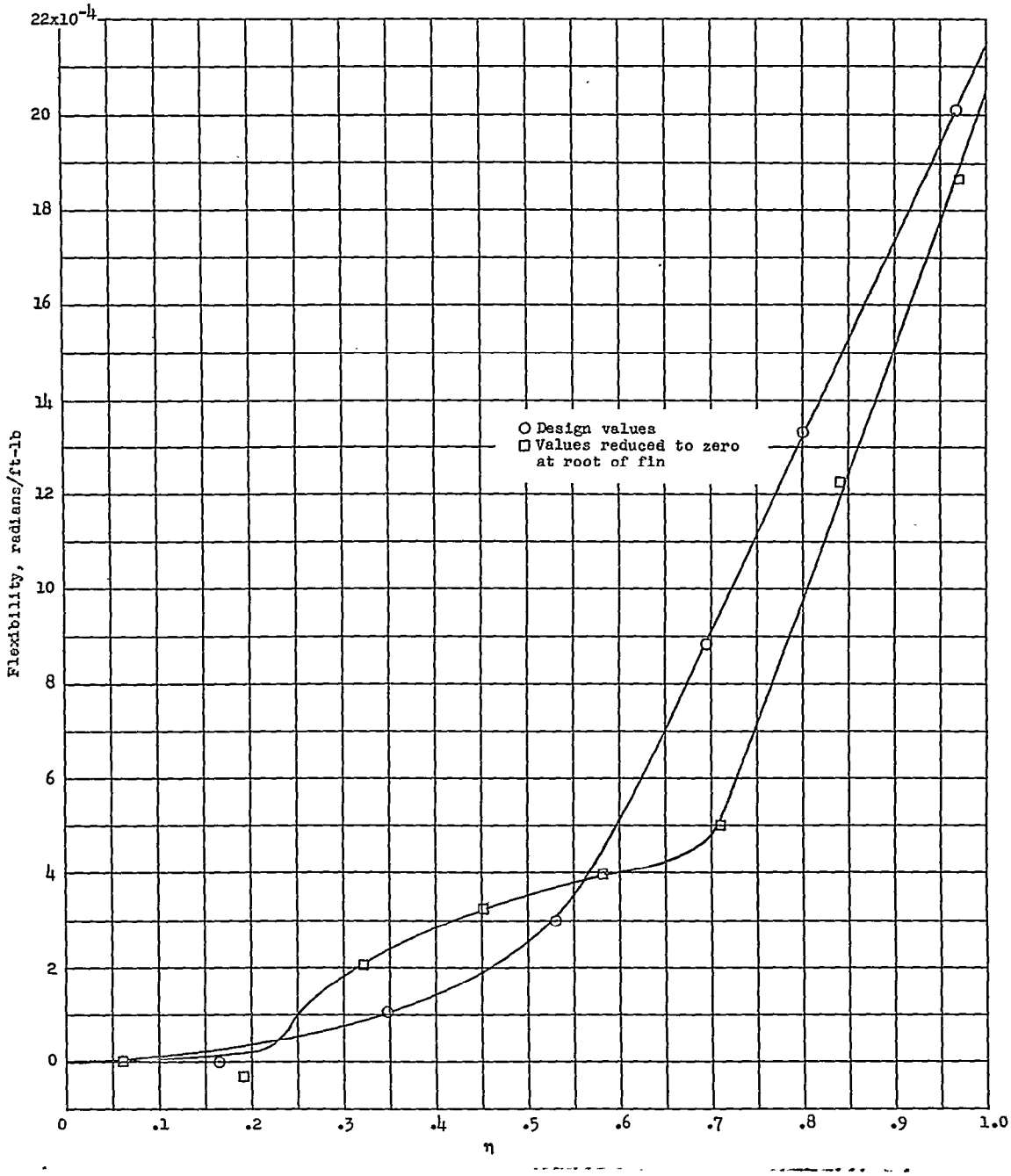

(c) Angular torsion deflection of fin per unit yawing moment applied to stabilizer, model 2.

Figure 6.- Continued.

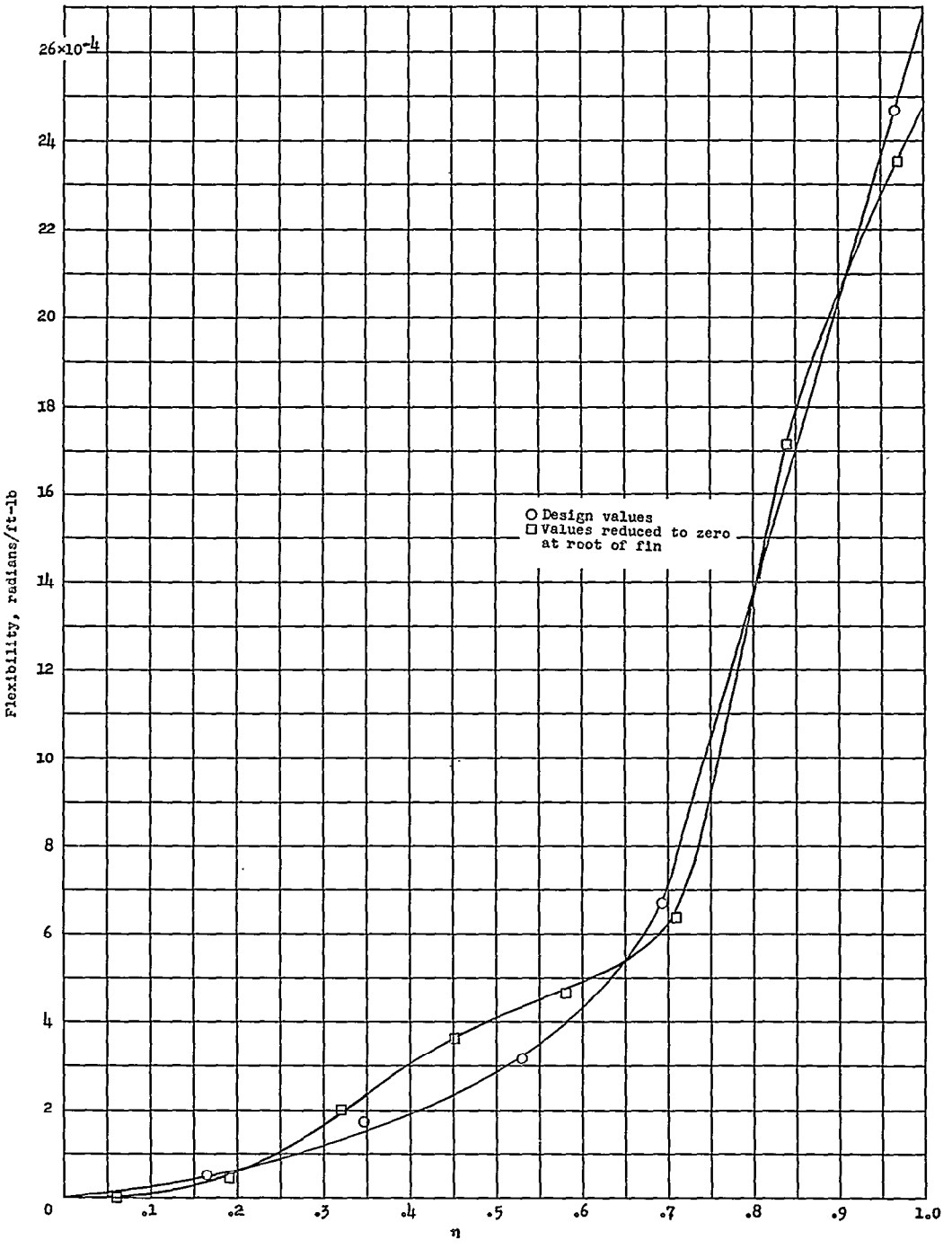

(d) Angular bending deflection of fin per unit rolling moment applied to stabilizer, model 2.

Figure 6.- Concluded.

[redacted]

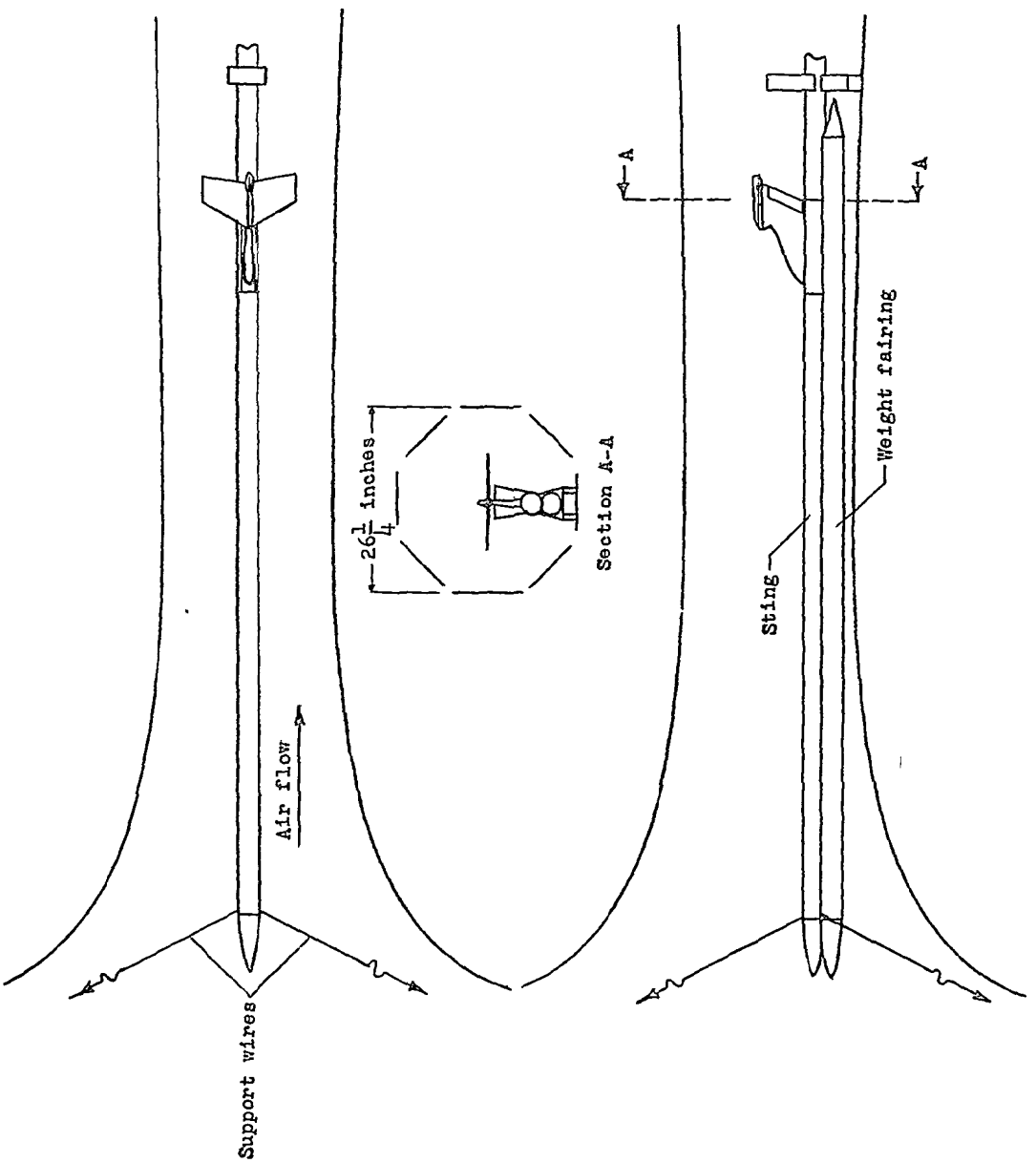

Figure 7.- Sketch of model mounted on sting and installed in tunnel.

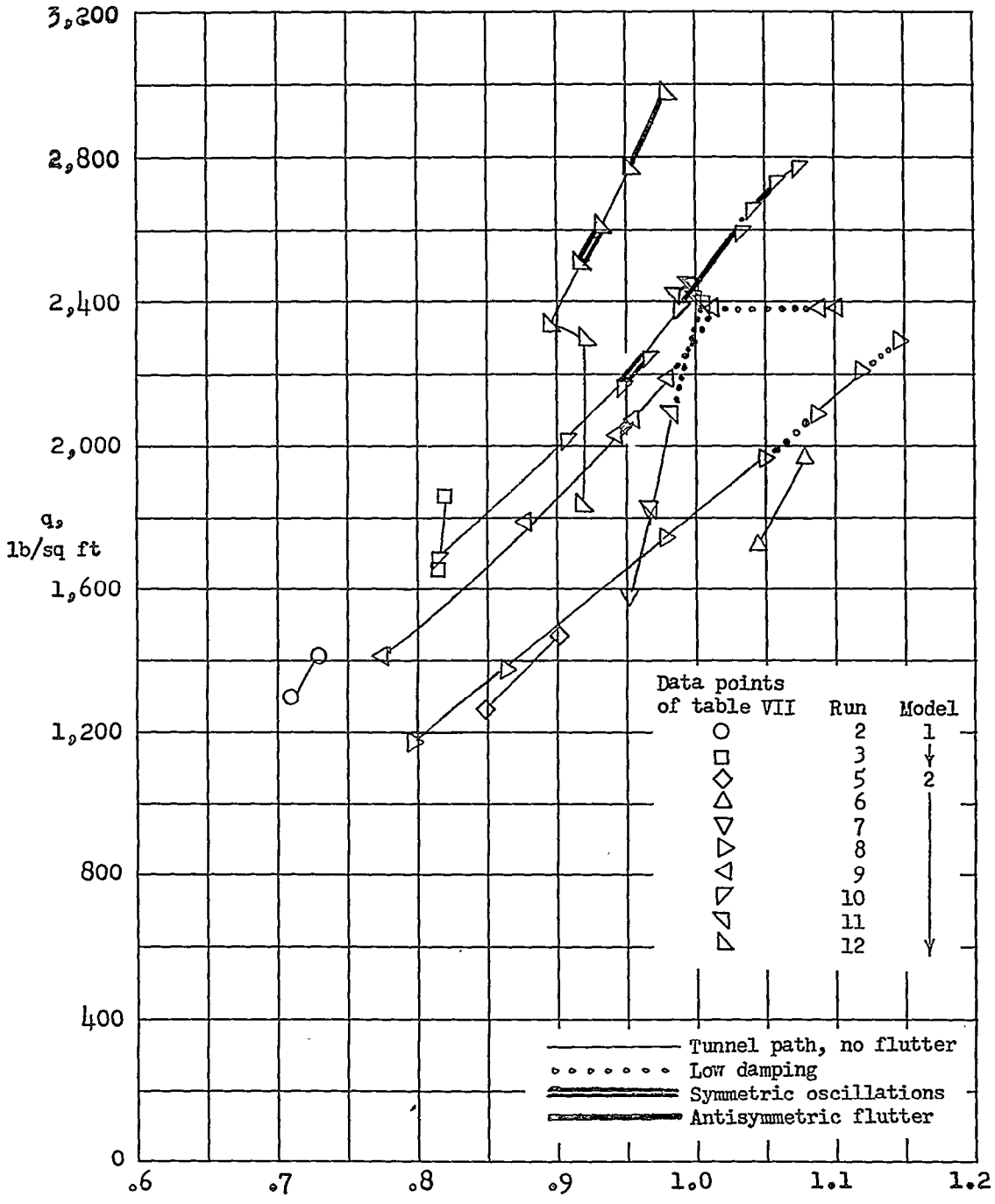
3,200
2,800
2,400
2,000
q,
lb/sq ft
1,600
1,200
800
400
0
.6
.7
.8
.9
1.0
1.1
1.2
Data points
of table VII
Run
Model
2
3
5
6
7
8
9
10
11
12
1
2
Tunnel path, no flutter
Low damping
Symmetric oscillations
Antisymmetric flutter

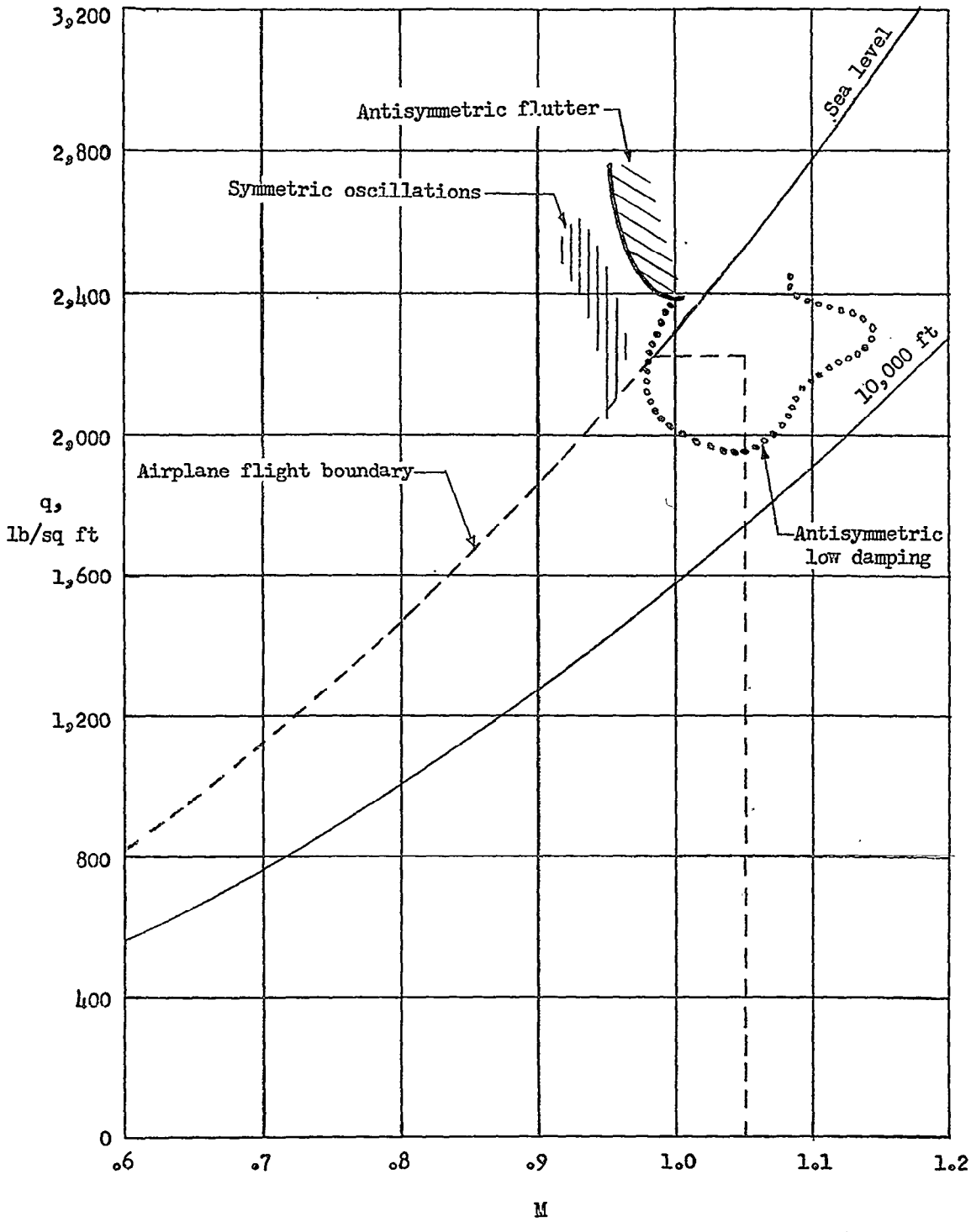

Figure 9.- Summary of flutter results.

PRELIMINARY TRANSONIC FLUTTER INVESTIGATION OF MODELS OF T-TAIL OF BLACKBURN NA-39 AIRPLANE

By George W. Jones, Jr., and Robert W. Boswinkle, Jr.

ABSTRACT

The models were dynamically and elastically scaled in accordance with criteria which include a flutter safety margin. The investigation is to be considered preliminary in that only estimated airplane properties were available for the scaling. The investigation was made in the Langley transonic blowdown tunnel and covered a Mach number range from 0.71 to 1.15.

INDEX HEADINGS

Airplanes - Specific Types	1.7.1.2
Aeroelasticity	1.9
Vibration and Flutter - Elevators and Rudders	4.2.2.1

[redacted]

PRELIMINARY TRANSONIC FLUTTER INVESTIGATION OF MODELS OF T-TAIL OF BLACKBURN NA-39 AIRPLANE

George W. Jones, Jr.

Robert W. Boswinkle, Jr.

Approved:

Eugene C. Draley
Chief of Full-Scale Research Division
Langley Aeronautical Laboratory

rh
(3/21/58)

[redacted]